

Random graph approach to multifunctional molecular networks

Ivan Kryven *, Jorien Duivenvoorden, Joen Hermans, and Piet
D.Iedema

University of Amsterdam,
Science Park 904, Amsterdam, The Netherlands

May 24, 2022

Abstract

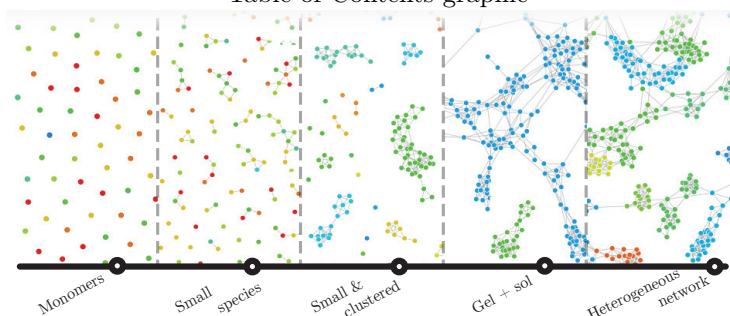
Formation of a molecular network from multifunctional precursors is modelled with a random graph process. The random graph model favours reactivity for monomers that are positioned close in the network topology, and disfavours reactivity for those that are obscured by the surrounding. The phenomena of conversion-dependant reaction rates, gelation, and micro-gelation are thus naturally predicted by the model and do not have to be imposed. Resulting non-homogeneous network topologies are analysed to extract such descriptors as: size distribution, crosslink distances, and gel-point conversion. Furthermore, new to the molecular simulation community descriptors are invented. These descriptors are especially useful for understanding evolution of pure gel, amongst them: cluster coefficient, network modularity, cluster size distribution.

*i.kryven@uva.nl

Tel.: +31 20 525 6423

Fax.:+31 20 525 5604

Table of Contents graphic



Nomenclature

α	constant related to chain stiffness and volume exclusion
a'	scaling factor for average shortest path
A	adjacency matrix
b_k	disconnected components of the network
c_e, c_i, c_m	reaction propensity coefficients
$c_k, c(A)$	local and global clustering coefficients
d_i	degree of node i
$d_{i,\text{free}}$	free degree of node i
$d_{i,\text{max}}$	maximum degree of node i
E_{max}	maximum number of edges in the network
f_i	concentration of fatty acids with i unsaturations
g_i	hindrance effect
$g_{01}(\chi)$	gel indicator function
$H(\chi)$	Heaviside function
k_p, k_c, k_m	reaction rate constants
l	average length of a chemical bond
n	number of nodes in the network
n_A	Avogadro number
N	number of samples in MC
$O(n)$	big O notation for asymptotic behaviour of a function
$p_{i,j}$	shortest path between nodes i, j

p	average shortest path
$P(A)_{i,j}$	probability of the next reaction between monomers i, j at given topology A
$P^*(A)_{i,j}$	proposal probability for the MCMC scheme
$\mathcal{P}(k)$	Poisson distribution
Q	stochastic matrix for computing steric hindrance
R	effective reaction distance
ρ	molar density
$s_1(q), s_2(q)$	Markov chain for MCMC sampling
$S_1(n), S_2(n)$	size of largest, and second largest components for an n -monomer system
t	reaction time
τ	waiting time between reactions
u_i	uniformly distributed random variable
$U[0, 1]$	uniform distribution
V	volume
W_n	concentration of TAGs of functionality n
$\Phi(\mathbf{A})_{i,j}$	cyclisation rate for nodes i, j
χ	conversion of edges
χ_g	Conversion at gel transition
z	current number of edges in the network

1 Introduction

Polymer science profits from the rapid development in the computing field in a very straightforward way: the complexity of macromolecular architecture or geometry is, to a growing extent, captured by simulation of the most basic physical processes. Instead of following heuristics leading to the classical mathematical equations. We anticipate that properties of continuum can be obtained as emerging from repeated simulations of the many-body physics at the nano-level, a strategy that seems to be more properly placed in stochastic simulations than in deterministic mathematical modelling. That said, one must realise that such simulations imply an enormous spread of length and time scales: even the simple case of a linear polymer exhibits geometrical structure from the scale of a chemical bond (1Å) to the scale of the gyration radius (100Å), and col-

lective length scales in dense materials often are even much larger. Moreover, our drive for modelling is not limited to linear polymers but also is directed at tree-like branched structures, cross-linked polymers, and even infinite molecular networks, *i.e. gels*. In this paper we propose a strategy that draws a consensus between what can be computed on the one hand and pursuing fundamental roots of the matter at hand on the other.

The process of assembly or polymerisation of molecular networks usually goes through a few temporal stages: disconnected monomers, linear polymer, branched polymer, and gel (an infinite network) [6, 8, 21]. Furthermore, the gel itself should not be perceived as a single, final state of polymer topology. After the gel point the connectivity patterns of the network continue to evolve[1, 40, 2]. In fact, in many cases a major part of the whole process of conversion may occur in the gel regime[23].

Side by side with new developments in Polymer Reaction Engineering, a novel field of *network science* has been introduced recently. In a much broader sense, the main object of studies in network science is networks regardless their background, *i.e.* not necessarily molecular networks. In chemistry, not surprisingly as chemical bonding leads to connectivity problems, one of the main toolboxes in network science, graph theory is already in use, for instance, in the form of the Wiener index [33]. However, apart from this line of research, the applicability of graph theory to large or infinite molecular networks, has received little attention. The current paper presents a cross dissemination between polymer science and network science as disciplines, with special care devoted to polymer-related issues. The problem we deal with in the present paper has three main features.

a) The functionality of the monomer is limited and satisfies a predefined frequency distribution. The monomer functionality is crucial for the gel formation and properties of the material[34, 27, 25]. A bi-functional monomer just forms linear chains. Monomers with higher functionality may lead to gels or infinite networks. Star macro-monomers may carry many functional groups, thus being a perfect base for complex molecular networks.

b) The average reaction rates may decrease by orders of magnitude due to diffusion limitation as a consequence of the decrease of the free volume caused by the

formation of the polymer network, *e.g.* as in Ref. [14]. The Trommsdorff or gel effects in radical polymerisation is an example of this. Moreover, the mobility of the larger molecules is affected more strongly than that of small molecules. This may affect the rates of reaction, depending on the type of molecules involved in those reactions. The issue of 'chain length dependent termination' is a frequently studied example of this phenomenon [19]. Furthermore, due to steric hindrance effect some monomers might be less available for the reaction being shielded by the surrounding topology of the network. The available polymerisation models accounting for shielding[11] have a mean-field nature and consequently do not allow for correct interpretation of possible inhomogeneities or irregularities present in network topology.

c) The topological distance between reacting units has to be accounted for. The distance between reacting units is not an issue in systems where these units make part of separate larger assemblies moving so fast that their average distance - or concentration - is the dominating factor. In large networks, however, the units are relatively fixed and more likely to react if the distance is small. In atomistic simulations position and reactivity are addressed by the 'capture sphere growth approach'[11]. In percolation theory monomer position and reactivity is described using a grid in 3D space. However, even without performing simulations in actual three-dimensional space, it is possible to incorporate geometrical information inferred from the network topology [20], from analytical results on random walks[7, 39, 9], or from population balance equations [24, 22].

Here, we present a new approach based on Random Graph Modelling, which must be considered as the first attempt ever in non-atomistic modelling, to account for all the three features described above. It is based on the kinetic Monte Carlo concept[38, 37, 28], where we explicitly deal with position-reactivity by using the graph-theoretical concept of the shortest path between monomer pairs. This is one significant step further than recent kinetic MC modelling studies, where the impact of size of individual (polymer) molecules on reactivity is accounted for [29]. In this paper we will show that this is an ambitious but still feasible approach, as it is not computationally very demanding. Given the fact that kinetic MC typically requires 10^9 to 10^{11} units to achieve statistically relevant results, one might expect that introducing the three features described

above would lead to excessively expensive calculations, but we will show that this is not the case. It is indeed the higher functionality of the monomers that creates a computationally very favourable condition concerning the required size of the domain simulated, typically 10^4 units.

This paper is structured as follows. To introduce the idea of application Random Graph Models to polymerisation problems, we explain the key concepts, such as: adjacency matrix, relation between topological and spatial distances, relation between steric hindrance and node centrality. Then, these concepts are used to build a Gillespie's stochastic simulation algorithm that describes evolution of network topology from monomers up to the full conversion of bonds. We also explain how the stochastic simulations can be accelerated applying the Markovian Chain Monte Carlo (MCMC) principle. Finally, the theoretical results are fortified with an extensive study on a realistic system: polymerisation of triacylglycerides, which is more commonly known as the 'drying' of oil paint. Simulation results include widely used in the reaction engineering community descriptors as, for example, size distribution, gel point conversion, distance between crosslinks. Furthermore, novel descriptors for molecular networks that are especially suitable for post gel region, are introduced. Among these descriptors: modularity of network, clustering coefficient, average path, and cluster-size distribution.

2 The model system

Star macromonomers Star polymers consist of a few arms joined together on one end [34]. The arms may carry multiple functional groups, (Figure 1), making star polymers a very attractive basis for construction of larger macromolecular networks. In the current paper we develop a model for polymerisation of macromonomers that are essentially star polymers of various functionality. Since in this study the focus is on the connectivity patterns of such monomers incorporated into a network, we will use terms monomer and node interchangeably, depending on the chemical or topological nature of the issue at hand. The monomers will be distinguished according to their functionalities $d_{i,max}$. A frequency distribution of functionalities is assumed to be known.

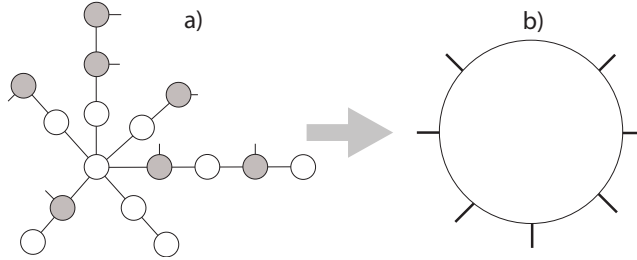


Figure 1: *a)* A schematic representation for the multifunctional macromonomer as a star polymer molecule. Shaded nodes carry free functional groups and thus provide means for further polymerisation into a complex network. *b)* Coarse representation for a monomer as a 'blob' retaining the number of functional groups.

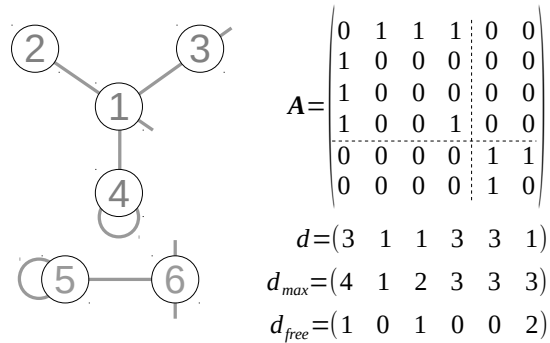


Figure 2: An example of a network model with 6 nodes, the corresponding adjacency matrix \mathbf{A} , and maximum degree vector d_{max} . There are six nodes in the system: nodes 4 and 5 have a loop; nodes 3,4,5 have all functionalities used, $d_{i,free} = 0$; nodes 1,3,6 have free functionalities available. The adjacency matrix \mathbf{A} is block diagonalised to emphasise the fact that there are two connected components in the system. The maximum number of edges is $E_{max} = 16$, and the current number of edges used is 12, or as a conversion fraction, $\chi = \frac{3}{4}$.

Graph representation of a molecular network In chemical context, graphs have been used to represent connectivity of (carbon) atoms in an organic molecule with a priori defined structure[17, 33]. Here, we represent the whole molecular system as a single undirected graph, regardless of the system composition: as disconnected monomers, ensemble of polymers, or a single connected network. Nodes numbered with index $i = 1, \dots, n$ represent monomers, and edges represent chemical bonds between such monomers. Each node can have at most $d_{i,max}$ edges. The adjacency matrix of the molecular network is defined as a square matrix,

$$\mathbf{A}_{i,j} = \begin{cases} 1, & \text{node } i \text{ has bond with node } j, \\ 0, & \text{no bond between } i \text{ and } j \end{cases} \quad (1)$$

The degree of node i may be lower than its maximum degree, so we distinguish between the maximum degree d_{max} (monomer functionality defined beforehand), the actual degree,

$$d_i(\mathbf{A}) = \sum_{1 \leq i \leq j \leq n} \mathbf{A}_{i,j} + \mathbf{A}_{i,i},$$

and the free degree,

$$d_{i,free} = d_{i,max} - d_i(\mathbf{A}).$$

The adjacency matrix \mathbf{A} together with the maximum degree $d_{i,max}$ constitute the model representation for a state of a particular molecular system. Figure 2 gives a simple example of a 6-monomer system and the corresponding matrix representation. In view of limitations posed on node's degree, $d_{i,max}$, the maximum number of edges in the whole network is also limited, $E_{max} \leq 0.5 \sum_i d_{i,max}$. The last equation becomes equality if $d_{i,max}$, $i = 1, \dots, n$ is a *graphic sequence*[10], namely: $\sum_i d_{i,max}$ is an even number, and for any $r \leq n - 1$, the following inequality holds,

$$\sum_{i=1}^n d_{i,max} < r(r-1) + \sum_{i=r+1}^n \min(r, d_{i,max}). \quad (2)$$

The graphic sequence is an important concept for finite simulation systems. Since the degrees of nodes are completely random (up to a specific frequency

distribution), it is useful to constrain the degree sequence of a finite simulation system to be graphic and thus eliminating small-size system effects that are not in an infinite network. This idea may be compared to imposing periodic boundary conditions in a simulation box for partial differential problems in order to avoid the effect of boundary layers.

Knowing a maximum number of edges allows defining a natural way of quantifying the polymerisation progress that evolves from 0 to E_{max} edges,

$$z = \sum_{i=1}^n d_i(\mathbf{A}), \quad z = 0, \dots, E_{max}, \quad (3)$$

or as a relative conversion $\chi = \frac{z}{E_{max}} \in [0, 1]$. Before proceeding to defining the principle of choosing a pair of nodes receiving a new edge on each polymerisation step, we need to introduce two concepts first: the idea of distance between nodes, and a measure of the node's centrality, which will allow us to address steric hindrance effects.

Topological distance The probability of a reaction between two monomers incorporated in the network is smaller if they are positioned far apart in space. Our model does not explicitly include spatial configurations, but certain information on the distance between any two nodes is encoded in the connectivity pattern defined by the adjacency matrix \mathbf{A} . The shortest path from node i to node j is the shortest sequence of intermediate nodes that link i, j together. The length of the shortest path is the number of edges in this sequence. If nodes i, j are adjacent then the shortest path is 1; if they do not belong to the same connected component then the path is defined to have length 0. While the shortest path $p_{i,j}$ does not explicitly tell us how far the nodes are in space, it sets an upper bound on the distance: the two nodes cannot be further apart than the shortest path times length of the edge, l . Later on, we will exploit this fact to develop a notion for network density. Let $p_{i,j}$ denote the shortest path between nodes i and j . One can always find such a path by applying a path-finding algorithm directly on the adjacency matrix A , for instance the Dijkstra algorithm[18]. In a finite network, the average shortest path,

$$p = \frac{1}{n \cdot (n - 1)} \cdot \sum_{i \neq j} p_{i,j}$$

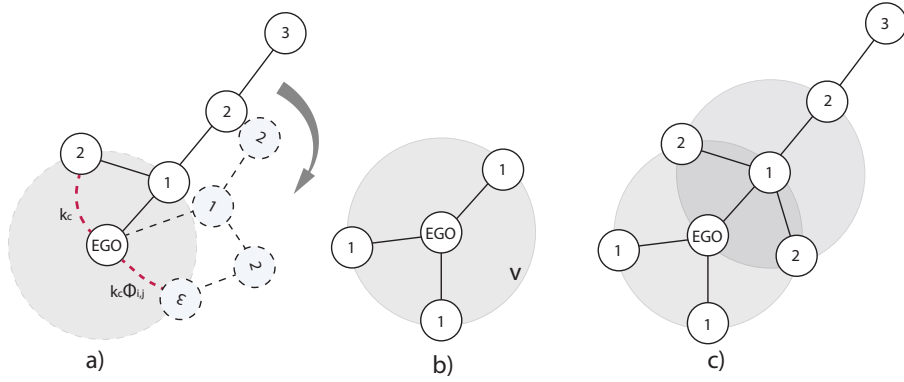


Figure 3: Network topology as seen from the perspective of a single node (marked as 'EGO'). Numbers indicate the shortest path distance to EGO. a) The reaction probability of two monomers incorporated in the network depends on the probability of the path configuration that brings these nodes together (b-c). Both the immediately surrounding and the more remote nodes contribute to the steric hindrance effect.

is proportional to the radius of gyration and hence there is a proportionality between the volume occupied by the monomer network and the volume of the gyration sphere: $\rho n = V \propto p^3$. Assuming a homogenous density of the network ρ , augmenting the number of nodes from n up to $a \cdot n$ will cause a scale-up of the average shortest path to $a' \cdot p$. The exact value of a' depends on spatial configuration of the monomers but the lower bound is given by

$$a' \geq \frac{\left(\frac{4}{3\pi} a \rho n\right)^{1/3}}{\left(\frac{4}{3\pi} \rho n\right)^{1/3}} = a^{1/3} \quad (4)$$

Thus, any polymerisation model has to respect the scaling ratio $\frac{a'}{a^{1/3}} \geq 1$, otherwise the produced topologies will not have any feasible spatial configurations. Even though this condition is necessary but not sufficient, it allows us to restrict ranges for input parameters for the model, post factum.

In order to formulate the reaction rate between two nodes incorporated in the network ($p_{i,j} > 0$), we will follow a similar reasoning. This time we additionally account for spatial configurations, assuming that the shortest paths can be mimicked by self-avoiding random walks. Two monomers need to be at min-

imal reaction distance R to allow reaction. For a sub-chain approximated by a random walk[26], the probability of two ends being at distance R is proportional to

$$\Phi^*(A)_{i,j} \left(\frac{3}{2\pi l^2 p_{i,j}} \right)^{3/2} e^{-\frac{3R^2}{2l^2 p_{i,j}}}. \quad (5)$$

Now, let us estimate the probability that a random walk is self-avoiding given that its end-to-end distance is R . We assume that all monomers are distributed uniformly in the gyration volume $V = ap^{3/2}$. Here a is a constant related to the stiffness of a polymer chain. Since the positions of all monomers $x_k = 0, \dots, x_p$ are distinct, the probability that position x_k does not coincide with all previous positions is $1 - k ap^{-3/2}$. Hence, the total probability that the whole chain is self avoiding is given by

$$\prod_{k=1}^p (1 - k ap^{-3/2}) \approx e^{-a p^{3/2} \sum_{k=1}^p k} = e^{-0.5 a p^{-3/2} (1+p)p} \approx e^{-\alpha p^{-1/2}}.$$

Note that a similar argument has been proposed by Flory[12]. Flory, furthermore, derived the value of α from measurable physical constants related to solvent properties, the stiffness of a chain, and monomer volume. Combining the last relation with (5) and taking $R = l$ gives the probability of a self-avoiding cyclic chain configuration,

$$\Phi(\mathbf{A})_{i,j} = C p_{i,j}^{-3/2} e^{-\frac{3}{2} p_{i,j}^{-1} - \alpha p_{i,j}^{1/2}}. \quad (6)$$

The constant C is chosen to satisfy $\Phi(2) = 1$ allowing to relate the intramolecular reaction rate constant to the propagation rate constant, as will be shown later on. Another constant appearing in (5), α , defines the rate of decline of the reaction probability, asymptotically at large distances. Note that $\Phi(\mathbf{A})_{i,j} = 0$ means that these nodes do not belong to the same connected component and that their spatial distance cannot be inferred from the topology. In this case the reactivity will be defined by a different mechanism based on the chemical rate constant and the degree of steric hindrance.

Steric hindrance as a centrality measure Here, we will construct a centrality measure, defined by numbers $g_i \in [0, 1]$ that will reflect how much a node is obscured by other nodes in the network, and thus experience a steric

hindrance effect. Matrix function $g(\mathbf{A})$ is set up according to three principles:

- 1) the nodes of higher degree are more obscured: if $d_i > d_j$ then $g_i < g_j$;
- 2) if the node is not obscured then $g_i = 1$; $g_i = 0$ means full obscuration;
- 3) from two nodes of the same degree, the node adjacent to a more obscured one is more obscured.

In order to satisfy the first principle it is sufficient to choose g_i proportional to $1/d_i$, which also has a logical interpretation from the excluded volume point of view (Figure 3b). The second principle might be achieved by an appropriate rescaling. It is only the third principle that requires to incorporate information on the specific topology A (Figure 3c). Altogether, the principles can be reformulated in the form of an implicit equation for the reciprocal $g_i^* = \frac{1}{g_i}$,

$$g_i^* = \lambda_i d_i \sum_{j \sim i} g_j^*, \quad (7)$$

where the summation is performed over all nodes j adjacent to node i , and λ_i is a normalisation factor required to ensure existence of the solution. The implicit equation (7) rewritten in a matrix form yields an eigenvalue problem,

$$g^* = Qg^*, \quad (8)$$

$$Q_{i,j} = d_i \sum_j \frac{A'_{i,j}}{\sum_k A'_{k,j} d_j}$$

Here matrix \mathbf{A}' coincides with \mathbf{A} except for the diagonal where $(\mathbf{A}')_{i,i} = 1$. Matrix Q has the same size and number of zero elements as the adjacency matrix \mathbf{A} . With no loss in generality we may consider $d_i > 0$ for all nodes (otherwise $d_i = 0$ would yield a trivial solution $g^* = g_i = 1$ due to the second principle). The eigenvalue problem as formulated in (8) is ready to use in the case of a fully connected network (*i.e.* gel). In the case of a few network components that are not connected to each other, \mathbf{A} has block-diagonal form. Solving the eigenvalue problem in each block of matrix \mathbf{A} would lead to a correct ranking within each separate component, but it would not allow to relate the extent of steric hindrance of two different components. To overcome this problem, we normalise g in each component of the network (each block of block-diagonalised \mathbf{A}):

$$g_i = \frac{\min_{i \in b_k} (g_i^*)}{g_i^*}, \quad i \in b_k,$$

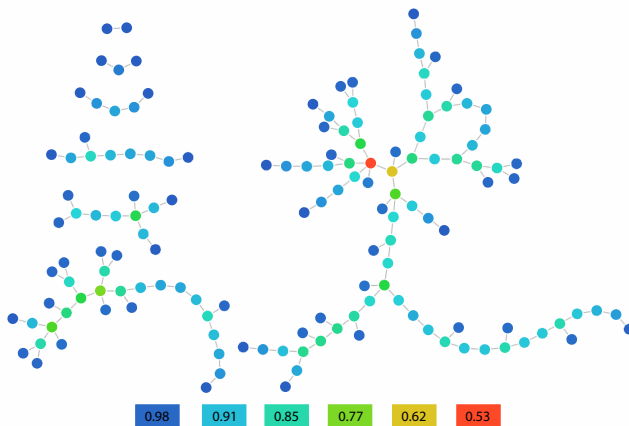


Figure 4: A sample of a network topology with values of steric hindrance factors, $g_i(A)$, indicated for each node. The example shows that $g_i(A)$ is defined by both the degree of a node and its position in the topology.

where $k = 1, \dots, m$ counts connected components b_k of the network \mathbf{A} . An example of a network topology with g_i computed for each node is given in Figure 4.

The fact that the matrix Q in the eigenvalue problem (8) is normalised, allows to alternatively view Q as a Markov (left-stochastic) matrix defining a random walk on the network[30]. Recall that $Q_{i,j} > 0$ if and only if $A_{i,j} = 1$, hence Q defines a weighted graph with the same edges as in A . From this perspective, we may view the solution g_i^* as a frequency node-visiting by the random walk on the weighted graph Q . This means that instead of solving the expensive eigenvalue problem (8), it is sufficient to consider a fixed point iteration $g^* = Qg^*$ starting with an arbitrary vector with all non-zero components .

3 Stochastic simulation

We consider the process of network formation (or polymerisation) as a stochastic process $\mathbf{A}(z)$, $z = 0, \dots, E_{max}$ starting from an empty adjacency matrix $\mathbf{A}(0)$ and taking it to a matrix with one edge $\mathbf{A}(1)$, and so on up to, finally, $\mathbf{A}(E_{max})$.

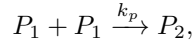
This evolution proceeds by means of sampling steps: matrix $\mathbf{A}(z+1)$ is obtained from matrix $\mathbf{A}(z)$ by placing an additional edge. Generally speaking, there are $E_{max} - z$ alternatives to decide where to put a new edge. This choice is performed according to a conditional probability accounting for all possibilities for the new edge to appear, obeying the reaction propensity coefficients c_e, c_i, c_m and given the topology \mathbf{A} ,

$$P(\mathbf{A})_{i,j} = \lambda_z \cdot \begin{cases} c_e d_{i,free} d_{j,free} \left(g_i(\mathbf{A}) g_j(\mathbf{A}) \right)^\beta & i \neq j, \Phi(\mathbf{A})_{i,j} = 0; \\ c_i d_{i,free} d_{j,free} \Phi(\mathbf{A})_{i,j}, & i \neq j, \Phi(\mathbf{A})_{i,j} > 0; \\ c_m \binom{d_{i,free}}{2}, & i = j. \end{cases} \quad (9)$$

Here the normalisation coefficient λ_z is selected to satisfy

$$\sum_{i,j} P(\mathbf{A}(z))_{i,j} = 1. \quad (10)$$

The first line of (9) refers to a new edge between nodes forming distinct components of the network (in the case of an intermolecular reaction, no path exists between i, j : $\Phi(\mathbf{A})_{i,j} = 0$). The probability $P(\mathbf{A})$ here is defined via the node's degree d_i and its steric hindrance factor g_i . The intermolecular propensity constant c_e is related to dimerisation rate, $c_e = \frac{2k_p}{Vn_A}$, where $V = \frac{n}{n_A \rho}$ denotes the reaction volume, and k_p is the usual rate constant for the reaction,

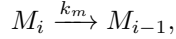


where P_1 denotes monomer, and P_2 dimer. The second line of (9) refers to a new edge between nodes from the same connected component (in case of an intramolecular reaction, a path between i, j exists: $\Phi(\mathbf{A})_{i,j} > 0$). The probability $P(\mathbf{A})$ incorporates the free degree of the nodes d_i and the probability that i, j are positioned close in space, $\Phi(\mathbf{A})$. The intramolecular propensity constant c_i is not dependent on volume this time, but it is directly equal to cyclisation rate constant k_c , according to the reaction equation,



where P_3 denotes a trimer, and P_3^c a trimer with a cycle. Finally, the third line of (9) refers to appearance of a loop (in graph theoretical sense), which represents a

reaction firing inside a monomer reducing its functionality by one. The sampling probability (9) is proportional to the combinatorial number of possibilities to select a pair of bonds out of the available free functionalities, leading to the binomial coefficient $\binom{d_i, free}{2}$. The propensity constant c_m is directly equal to reaction rate constant k_m in



where M_i denotes an i -functional monomer.

Gillespie’s algorithm The basis of Gillespie’s algorithm is formed by the concept of the homogeneous Poisson process, that counts reaction events occurring at rate λ . In this process, the number of events occurring in a time interval $(t, t + \tau]$ follows a Poisson distribution with an associated parameter $\lambda\tau$,

$$\mathcal{P}(k) = \frac{e^{-\lambda\tau}(\lambda\tau)^k}{k!}.$$

Thus, the waiting times between events are distributed according to

$$p(\tau) = \mathcal{P}(0) = e^{-\lambda\tau}. \quad (11)$$

Gillespie proposed a stochastic simulation algorithm (SSA), where an exponential distribution (11) is used to estimate the time intervals between reaction firings [13]. In the SSA the event rate is not constant but depends on the reaction propensity λ_z , (in the current case introduced in (10)). The actual time between the start and stage z is a sum of z waiting times:

$$t(z) = - \sum_{i=1}^z \frac{\ln(u_{i,0})}{\lambda_i}, \quad u_{i,0} \sim U[0, 1] \quad (12)$$

where $u \sim U[0, 1]$ refers to a uniformly distributed random variable. Therefore, the reaction time $t(z)$ is a random variable itself, that is determined by z samples from a uniform distribution.

On every stage of the reaction z , a pair of nodes i, j is selected to receive an edge according to the probability distribution $P(\mathbf{A})_{i,j}$, given in (9). Each of these selections is uniquely defined by two uniformly distributed random variables, $u_{z,1}, u_{z,2} \sim U[0, 1]$. This implies that the adjacency matrix at stage z

is uniquely defined by a specific sampling history. More precisely, the adjacency matrix A on stage z can be put into a bijective correspondence to a $z \times 2$ matrix that defines samples on the preceding stages:

$$\mathbf{A}(z) = F(\mathbf{U}), \mathbf{U} = \begin{pmatrix} u_{0,1} & u_{0,2} \\ u_{1,1} & u_{1,2} \\ \dots & \dots \\ u_{z-1,1} & u_{z-1,2} \end{pmatrix}. \quad (13)$$

This reflects the usual idea behind Monte Carlo simulations that all networks $F(U)$ for all sample matrices U are considered as equiprobable. Consequently, any statistical property (*e.g.* average degree, component size distribution, density) of the network $\phi(\mathbf{A})$ may be determined by an integration over the set of sampling variables $\Omega = [0, 1]^{2t}$. If independent sampling matrices U were drawn N times, the integral is approximated by a sum, the Monte Carlo estimator:

$$\int_{\Omega} \phi(F(\mathbf{U})) du \approx \frac{1}{N} \sum_{i=1}^N \phi(F(\mathbf{u}_i)). \quad (14)$$

Here, U_i , $i = 1, \dots, N$ are randomly generated instances of matrix (13). The error of estimator (14) decreases asymptotically as $N^{-\frac{1}{2}}$ when $N \rightarrow \infty$.

Markov Chain Monte Carlo, simulation of a large system The stochastic simulation that has been described above, proceeds by drawing samples distributed according to the two-dimensional probability distribution $P(\mathbf{A})_{i,j}$ given in (9). This can be done by drawing two successive samples from one-dimensional distributions. The first sample, s_1 , is drawn from the marginal distribution $\sum_{i=1}^n P(\mathbf{A})_{i,j}$; the second, s_2 - from the conditional probability distribution $P(\mathbf{A})_{s_1,j} \left(\sum_{j=1}^n P(\mathbf{A})_{s_1,j} \right)^{-1}$. This procedure requires recomputing all entries of the matrix $P(\mathbf{A})_{i,j}$, which is computationally the most expensive step of the whole algorithm. Observe, that even though the adjacency matrix \mathbf{A} is very sparse, matrix $P(\mathbf{A})_{i,j}$ with its upper bound on density E_{max}/n^2 , is a full one.

The computational cost of the algorithm may be significantly reduced utilising a Markov Chain Monte Carlo (MCMC) algorithm, which is also commonly

used in statistical mechanics and other disciplines. The MCMC algorithm replaces the draws by a specific Markov process having $P(\mathbf{A})_{i,j}$ as the stationary distribution [5]. More specifically, for a fixed matrix $\mathbf{A}(z)$, we design a sequence of pairs $(s_1(q), s_2(q))$ that is initiated by two random numbers from $1 \dots, n$. The transition from pair q to $q+1$ is realised according to the following principle:

$$(s_1(q+1), s_2(q+1)) = \begin{cases} (s_1^*(q), s_2^*(q)), & \text{if } u(q) < \min\left(\frac{P_{s_1^*(q), s_2^*(q)}}{P_{s_1(q), s_2(q)}} \frac{P_{s_1(q), s_2(q)}}{P_{s_1^*(q), s_2^*(q)}}, 1\right) \\ (s_1(q), s_2(q)), & \text{otherwise} \end{cases} \quad (15)$$

where $u(q) \sim U[0, 1]$, and $(s_1^*(q), s_2^*(q))$ is drawn from the proposal distribution $P^*(\mathbf{A})$. The proposal distribution coincides with the original $P^*(\mathbf{A})_{i,j} = P(\mathbf{A})_{i,j}$ when $i = j$, and assumes a simpler form for $i \neq j$,

$$P^*(\mathbf{A})_{i,j} = \lambda^* \cdot \begin{cases} c_e d_{i,free} d_{j,free} \left(g_i(\mathbf{A}) g_j(\mathbf{A})\right)^\beta & \text{intermolecular;} \\ c_i d_{i,free} d_{j,free}, & \text{intramolecular, } i \neq j; \\ c_m \binom{d_{i,free}}{2}, & i = j. \end{cases} \quad (16)$$

Although the MCMC scheme (15) provides only a means of approximate sampling, it possesses one very important feature: it is not necessary to compute all the elements of matrix $P_{i,j}$ but only certain selected values. This feature allows to considerably save on computational resources for large adjacency matrices.

The downside of MCMC is that one has to ensure that the Markov chain (15) operates in a stationary regime before terminating it and accepting the final values as a random sample that mimics samples from $P_{i,j}$.

4 Discussion/application to linseed oil network

In this section we discuss the kind of information one may extract from the random molecular networks generated by the stochastic simulations using the Random Graph Model as introduced above. The results are formulated as graph-theoretical properties that may be calculated with the MC estimator (14). These data are useful in improving our understanding of the system, but also might be used for physical interpretation of the topological information and its influence on the observable and measurable properties of the final material.

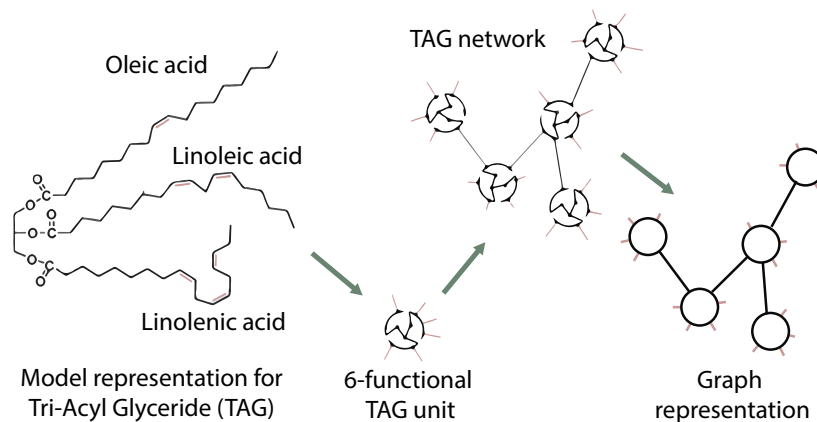


Figure 5: Conceptual model for representation of the linseed oil network. Triacyl glyceride is treated as a single node. Depending on composition of the nodes, they may have maximum functionality ranging between 0 and 9.

In order to demonstrate the RGM approach on a practical case we consider linseed oil polymerisation, which is more commonly known as the 'drying' of oil paint. The binding medium linseed oil consists of triacylglycerides (TAG) and the unsaturated groups on the three fatty acid (C19) chains cause the TAG-units to polymerise into a network. This curing process is a complex process involving radicals, oxygen, peroxides, etc., which is only partly understood, and only little quantitative kinetic information is available [16]. Here, we simplify this complex process to the coupling of the TAG-unit star monomers according to an estimated 'chemical' coupling rates, k_c and k_p , which then is affected by decreasing functionality, distance within the network and steric hindrance as is now possible with the RGM model. We expect that this model with strongly simplified kinetics will nevertheless contribute to a basic understanding of the linseed oil network, as influenced by its curing behaviour, but also by degradation, for instance by hydrolysis of the ester bonds. The conceptual model of TAG-unit network is illustrated in Figure 5. TAGs contain double bonds that are responsible for the formation of the cross-links. Since there can not be more than 3 unsaturations per fatty acid in the TAG node, the maximum number of connections node i can form is limited to 9, $0 \leq d_{i,max} \leq$

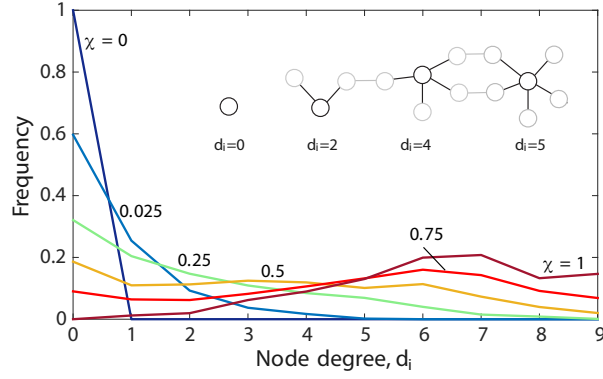


Figure 6: Evolution of degree distribution during polymerisation. Fraction of edges, $\chi \in [0, 1]$, depicts the progress of the stochastic process. The final distribution at $\chi = 1$ coincides with distribution of TAG-unit functionalities in linseed oil.

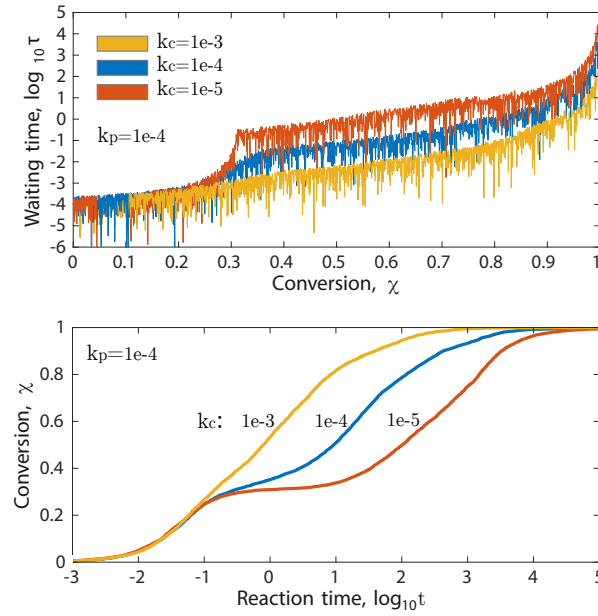


Figure 7: (Top:) time span between reaction events as a function of the conversion. (Bottom:) the conversion of edges versus total reaction time.

9. More precisely $d_{i,max}$ are distributed according to frequency distribution $W_n = \sum_{i+j+k=n} f_i f_j f_k$, $n = 0, \dots, 9$, where f_i denotes concentration of fatty acids with i unsaturations. The frequency that we have assumed in this study is based on the natural abundance of oleic, linoleic and linolenic acid in linseed oil, having, respectively, one, two and three unsaturations (see Figure 5). From the point of view of a single node the polymerisation process looks simple: the degree of each node, d_i , will transit from 0 to, eventually $d_{i,max}$. Thus the evolution of the frequency distribution of node degrees,

$$f_{i,degree}(\mathbf{A}) = \frac{1}{n} \sum_{j=1}^n \delta(d_j(A) - i).$$

has a simple form: in the beginning of the polymerisation process the distribution describes disconnected monomers, $f_{i,degree}(\mathbf{A}(0)) = 0, i > 0$, and $f_{0,degree}(\mathbf{A}(0)) = 1$. At the full conversion the distribution of node degrees approaches the distribution of functionalities of pure monomers (Figure 6).

The global properties of the network have less trivial dynamics. In order to extract various network properties we simulated ensembles of 10^4 monomers and averaged the results over 100 of such ensembles. These global properties in turn affect reactivity rates and the overall kinetics of the system. Even the timing of reaction events, given in (12), strongly depends on the ratio of rate constants k_c/k_p . For time intervals between the reaction events and the overall conversion/reaction time plot see panels in Figure 7. Alternatively, instead of increasing k_c/k_p , one may consider to decrease concentration of monomers, which by enhancing cyclisation has an identical effect on the system.

Gel transition Polymerisation of multifunctional monomers is known to pass through the gel transition: a transition that drastically affects the physical properties of the material. The gel point is experimentally well observable due to considerable differences in the material properties between the gel and sol phases, such as solubility and viscosity [4]. Hence, it is a common practice to define the gel transition point as a point where the observable properties change. Here, we will define the gel transition entirely on topological properties of the corresponding graph. Let's consider a sequence of adjacency matrices $A(n)$ constructed for identical input parameters and given number of nodes, n .

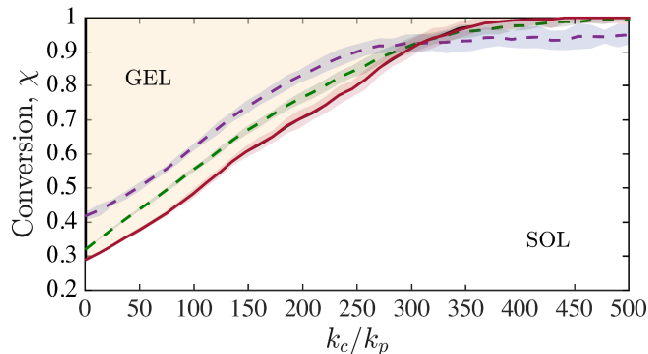


Figure 8: Gel point conversion as a function of reactivity ratio as obtained from the RGM simulation, confidence interval for $p = 0.95$. The dashed lines indicate the point when the average shortest path length is maximum.

We associate the gel part of the network with the giant component (in the sense of random graph theory [36]). Thus, the gel point is the time instant in the reaction progress at which the giant component emerges. More specifically, the largest component in the network is called gel if its size $S_1(n) = O(n)$ when n approaches infinity. Furthermore, if gel is present, the size of the second largest component is $S_2(n) = O(\log(n))$. In the pre-gel regime both $S_1(n)$ and $S_2(n)$ are equal to $O(\log(n))$. Thus distinguishing between pre- and post-gel regimes is equivalent to distinguishing between two asymptotical modes of $S_2(n)/S_1(n)$ when $n \rightarrow \infty$. We use this asymptotic estimates to determine whether the system operates in the gel regime for a given progress of the reaction z (or conversion χ),

$$g_{01}(\chi) = \begin{cases} 0, & \text{if } S_2(n)/S_1(n) \rightarrow \text{const} \\ 1, & \text{if } S_2(n)/S_1(n) \rightarrow 0 \end{cases}$$

where $S_1(n)$ is the size of the largest component for a system with n monomers and z edges, and $S_2(n)$ - size of second second-largest component. Clearly, $g_{01}(\chi)$ itself is a random variable and its mean has to be estimated by the MC estimator. When the number of samples in the MC estimator N becomes large, the gel indicator function $g_{01}(\chi)$ approaches the Heaviside function $H(\chi - \chi_g)$, where χ_g is a 'breaking point' separating the pre-gel and gel regimes. In practice,

for a fixed N , we identify χ_g by solving a least-squares problem that minimises the residual $\int_{\chi} |H(\chi - \chi_g) - g_{01}(\chi)| d\chi$.

The gel point conversion χ_g is plotted versus k_c/k_p in Figure 8. A clear discontinuity can be seen: the fraction equals to 0 up to the gel transition. Higher levels of k_c/k_p postpone the gel transitions up to the point when gelation does not occur at all. This is a logical result, since a higher k_c implies a stronger intramolecular cross-linking, which obviously competes the gel formation.

Molecular sizes As shown in Figure 7 the reaction rates are not constant, but slow down in a non-linear fashion. One of the causes for this effect is the emergence of large, connected components that restrict their internal monomers in reactivity. Molecular sizes in terms of number of monomers are equal to the number of nodes in connected components of the network that are not connected to each other. It is straightforward to identify the connected components of a graph in linear time using, for instance, breadth-first search[18]. Figure 9 shows how the distribution of sizes of these components (molecular size distribution) evolves in time.

Eventually, a connected component of the same order of magnitude as the whole network emerges (the giant component). The point in time/conversion when this event takes place marks the usual gel transition. The size of the giant component increases rapidly as it becomes connected to the rest of the components. Reactions between large components (including the giant component) dominate over reactions between small-sized components. This is why the size distributions in Figure 9 shifts back towards the origin after the gel transition. Thus, one observes that the gel point detected from the topology alone, as explained above, indeed marks the turning point of the size distribution. For high values of k_c/k_p the gel transition is postponed up to the full conversion (Figure 9b) or does not happen at all (Figure 9c). According to the general convention the data presented in Figure 9 excludes the giant component itself as it only refer to the sol part. In a complementary fashion, the fraction of nodes incorporated in the giant component is given in Figure 10.

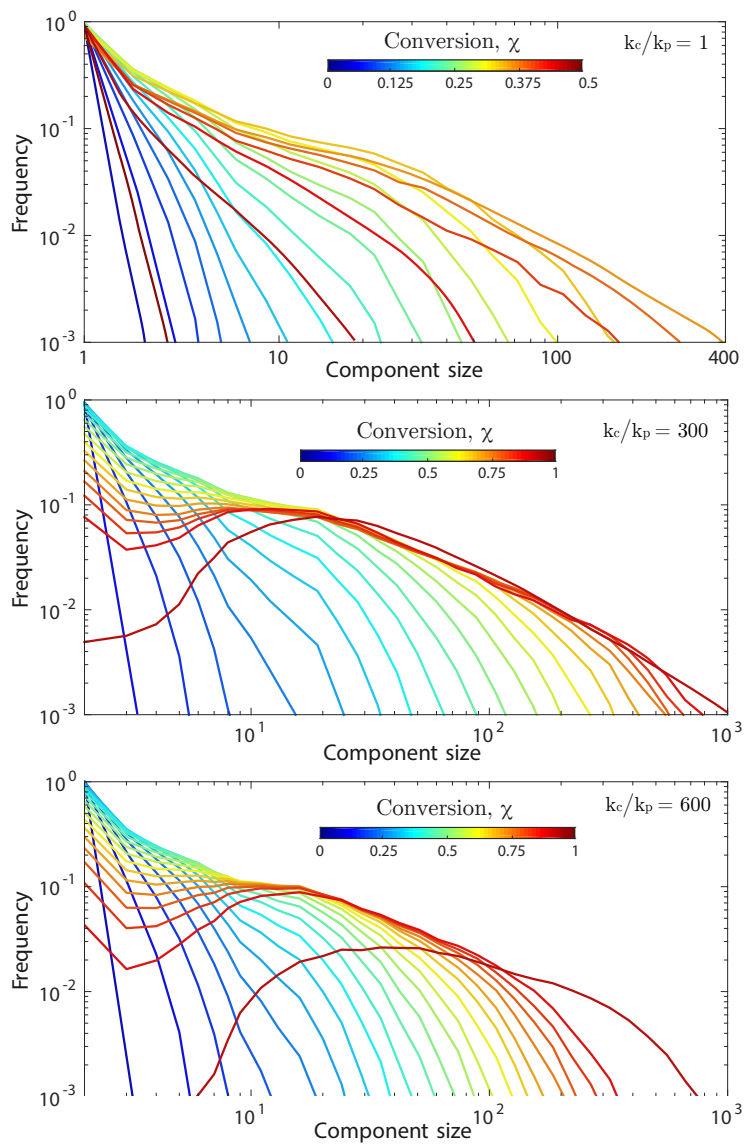


Figure 9: Evolution of size distributions (excluding gel) for three values of k_c/k_p .

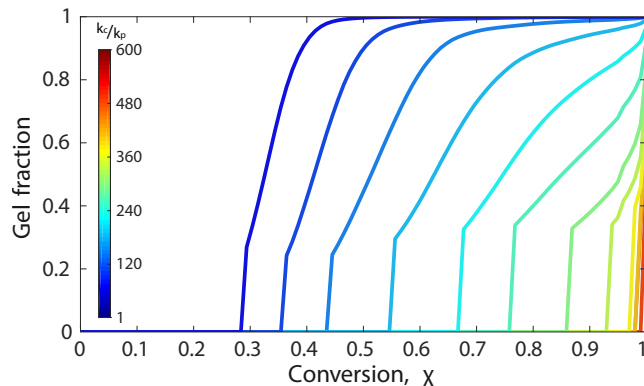


Figure 10: Fraction of monomers involved in giant component (gel) as a function of conversion for various values of k_c/k_p .

Structure of the network The characterisation of the polymer network in terms of numbers and sizes of connected components is a widely used in the polymer community. However, in cases where the topology is not a priori known (*e.g.* linear or regularly branched polymers), we have to invent new characteristic measures to describe how individual monomers are arranged inside the single connected component that the network eventually becomes. Although being randomly interconnected, the nodes may occasionally line up into certain *motifs* of special interest. The search for motifs that are frequently occurring in the network is a new structural characterisation method that is easy to quantify. For instance, the degree distribution is nothing else than the frequency of nodes having zero, one, two, etc., adjacent nodes.

Besides structural information, the size distribution of linear fragments plays an important role in the elasticity of polymeric networks [15, 32]. The number-average length of linear fragments strongly depends on the conversion; it increases at early stages of the reaction and eventually decreases to almost to 1. High values of k_c/k_p are associated with shorter linear fragments at intermediate stages of conversion, but ultimately, with longer linear fragments at later stages (Figure 11).

Another motif-related property is the local clustering coefficient. For node k , it is equal to fraction of pairs connected to k that are also connected to each

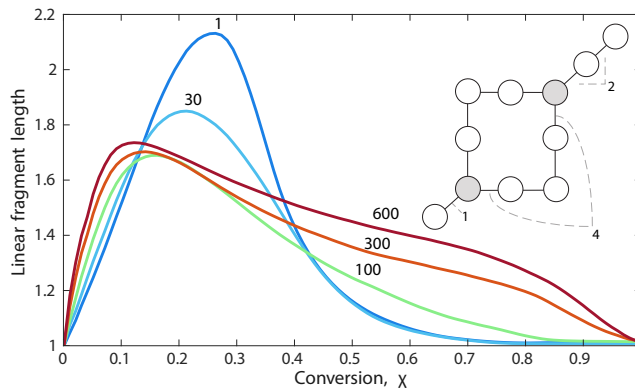


Figure 11: Average length of linear fragments as a function of conversion for various values of k_c/k_p . The illustration depicts a sample network with four linear fragments of lengths: 1, 2, 4, 4.

other(*i.e.* forms a triadic clousure),

$$c_k(\mathbf{A}) = \frac{\sum_{i < j} \mathbf{A}_{i,j} \mathbf{A}_{i,k} \mathbf{A}_{j,k}}{d_k(d_k - 1)}.$$

This coefficient is a number between 0 and 1, see the example of Figure 12. In order to transit from local clustering per node to average clustering of the whole network we apply averaging \mathbf{A} , $c(\mathbf{A}) = \frac{1}{n} \sum c_k(\mathbf{A})$.

The average clustering coefficient gives a good idea of small scale patterns that may arise in the network. At the beginning of the polymerisation, the average clustering increases monotonically in time. For systems with low values of k_c/k_p the average clustering becomes significant only in the gel regime. It is interesting to note that the average clustering decreases at conversions close to 1. This effect is caused by steric hindrance in the ultimately overcrowded network that eventually suppresses clustering.

Average path length The average path length of a network is a concept that defines the average number of steps along the shortest paths for all possible pairs of network nodes,

$$L(\mathbf{A}) = \frac{1}{n(n-1)} \sum_{i \neq j} p_{i,j},$$

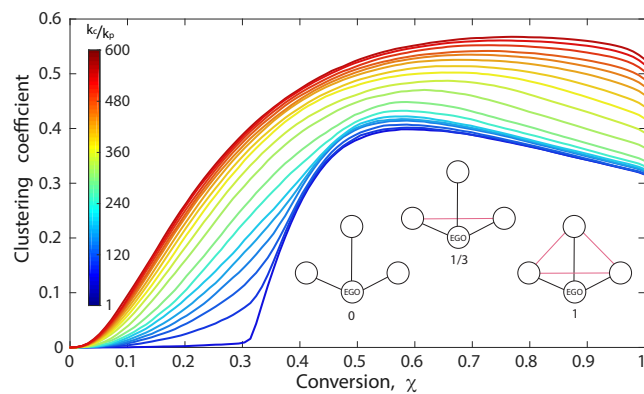


Figure 12: Clustering coefficient as a function of conversion for various values of k_c/k_p . Three examples of a 4-node network are given. The clustering coefficient of the node marked 'EGO' is equal to 0, $1/3$, or 1 depending on the connections between EGO's neighbouring nodes.

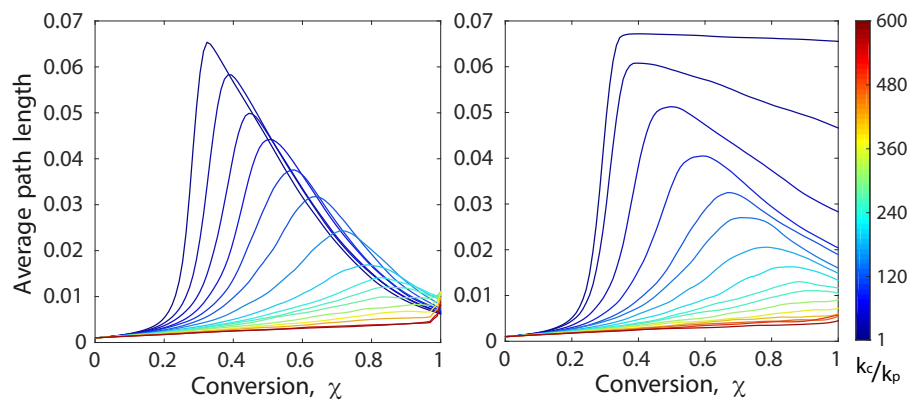


Figure 13: Average path length as a function of conversion. Left panel depicts results in the case of no intramonomeric reactions, right panel - high intramonomeric reaction rate ($k_i/k_p = 10$).

Here, $p_{i,j}$ denotes the distance between nodes i and j in network \mathbf{A} , if the nodes i, j are not connected, $p_{i,j} = 0$. One may think of average path length as a measure of 'network density'. Various theories connect the shortest path to observable data related to light scattering, radius of gyration, etc. [33]. Figure 13 shows how the normalised average path length evolves during reaction progress for various values of k_c/k_p . Note that even though the average path length is normalised by dividing by the total number of nodes n , it still depends on n and special care has to be taken, when comparing the average path lengths of two systems of different size. The two panels presented in Figure 13 represent cases with and without intramonomeric reaction. A pattern that is typical for many polymer properties, can be seen: the average path increases in the pre-gel regime and decreases thereafter. However, closer investigation reveals that the maximum of the average path does not exactly coincide with the gel transition but is shifted. This is demonstrated by Figure 8, where the conversion at maximum average path length and at the gel point is plotted for various values of k_c/k_p . The intramonomeric reaction leads to a more sparse network by consuming functional groups, and thus, reducing functionality of the monomers. Since the intramonomeric reaction is not hindered by the resulting topology, the influence of this reaction is most visible after the gel transition that is reflected by a suppressed decrease of the average path length (see Figures 13,8).

Structural non-homogeneity The evolving structure of networks may be more or less homogeneous, for instance microgels may (temporarily) evolve as a form of heterogeneity[35, 3]. It turns out that structural non-homogeneity is an inherited property of the polymerisation models that account for distance between monomers. Certain values of input parameters lead to topologies that, although being connected, can be partitioned into distinct clusters, comparable to microgels. These clusters are loosely connected between each other but are densely interconnected within themselves. This effect can be achieved when cyclisation dominates propagation (high values of k_c/k_p). For example, in diluted systems the chance that a monomer will connect to its direct neighbour (or another node from the same component) is higher than the chance of encountering a disconnected component. One way to measure the degree of inhomogeneity

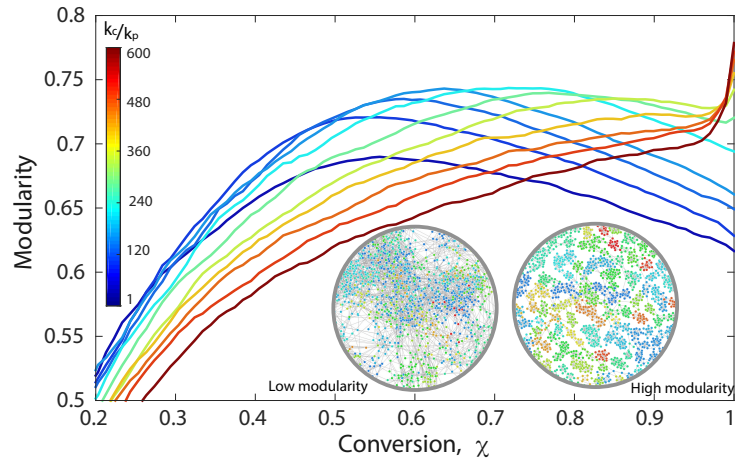


Figure 14: Modularity as a function of conversion for various values of k_c/k_0 . The two samples depict networks with low/high modularities.

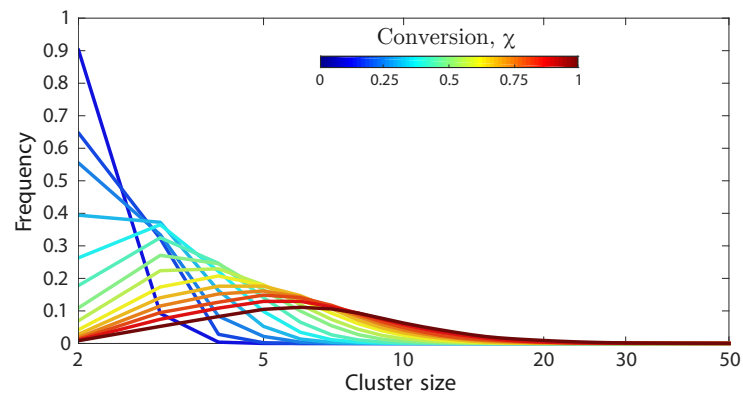


Figure 15: Cluster size distribution for various levels of conversion

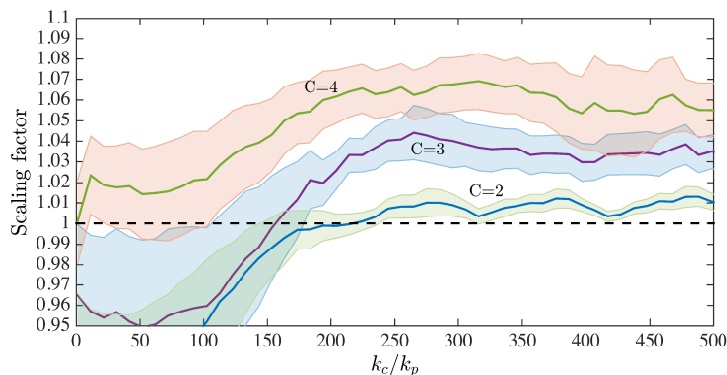


Figure 16: Scaling fraction vs k_c/k_p as obtained for three values of chain stiffness constant, α . The bands represent 0.9 confidence interval around mean value based on Monte Carlo sampled data.

(clustering) present in the network is the measure of *modularity*, which may be calculated using a special optimisation algorithm involving the adjacency matrix [31]. The evolution of modularity as presented in Figure 14 exhibits the increase-decrease pattern with a maximum at intermediate levels of conversion. High values of k_c/k_p postpone the maximum towards the full conversion, up to the point where the modularity increases over the whole time span of the process. It can be observed that a certain degree of structural inhomogeneity is prevalent even for very low values of k_c/k_p at intermediate conversions. However, at the final conversion a structure with distinct clusters is preserved only for high values of k_c/k_p .

As similar to the component size distribution, we may consider a cluster size distribution that evolves over time with reaction progress (Figure 15). Even though the value of k_c/k_p defines how well separated the clusters are, it has little effect on cluster sizes. However, cluster sizes are strongly affected by excluded volume constant α , that appears in (6).

Scaling The average path length is related to the gyration radius of individual molecules and to the density of the gel in space. The scaling of the average path length for gel networks has to satisfy the inequality (4). Testing this inequality for various values of input parameters helps to narrow down the range of valid

values for these parameters. Figure 16 shows the normalised scaling factor $\frac{a'}{a^{1/3}}$ of the final topology ($\chi = 1$) as a function of k_c/k_p . Low cyclisation to propagation ratios lead to topologies that possess a scaling factor under critical level, which implies that they are too dense to become embedded in a three-dimensional space.

Timeline of network topology Even though the final degree distribution of the monomers is fixed, various input parameters yield a vast range of different network topologies. We will now comment on the complex process assembling these topologies by highlighting a few important stages. The input parameters influence the positions of these stages in time/conversion but the order remains unaltered. In all cases the polymerisation obviously starts with all nodes disconnected, $d_{free} = d_{max}$ (see Figures 17-I and 18-II). We now separately consider scenarios for weak (k_c/k_p is small) and strong (k_c/k_p is high) cyclisations. When cyclisation is weak, shortly after the start of the polymerisation, many small disconnected components with tree-topology are formed (Figure 17-II). The sizes of the components increase but remain $o(n)$; the average length of the linear fragments continues to increase until it reaches the global maximum (Figure 17-III). The giant component of size $O(n)$ emerges, while cycles start to appear in all components (Figure 17-IV). These cycles remain being short and consequently do not considerably affect the average shortest path length. As the network is becoming more dense, long cycles start to appear occasionally. These long cycles seem to force the average shortest path length to start declining (Figure 17-V). As the density of the network continues to increase, modularity reaches its maximal value: clear structural non-homogeneity is present. (Figure 17-VI). At the full conversion the network consist of a single connected component. The last reactions, even at very low rates, connect the previously formed clusters and thus reduce the non-homogeneity. The final network is quite dense and homogeneous (Figure 17-VII).

Whereas in the case of strong cyclisation, small molecules with many cycles form shortly after the start of the reaction (Figure 18-II). The disconnected components grow in size for a much longer span of conversion before gel transition is achieved. Most of the new edges appear inside the connected compo-

nents, enhancing the clustering coefficient (Figure 18-III). The giant component emerges at a relatively high conversion and it has a non-homogenous structure. (Figure 18-IV). Finally, at the full conversion the major part of the network is occupied by the giant component, although other components of small size, $o(n)$, remain present too. The structure is highly non-homogenous. The full conversion is also the point at which the modularity and the average shortest path length reach maximum values.

Role of excluded volume principle An important and distinct feature of the RGM approach is that reaction rates depend on distances between monomers that are not known directly, but are implicitly inferred from the topological configuration of the network. In order to define the connection between topology and physical distance we employ the 'random walk' concept. The question arises, which of the random-walk models should be chosen: the commonly used random coil model, Φ^* as given in (5), or the self-avoiding random walk (excluded volume principle Φ , Equation 6)? A further question is: how would accuracy be improved in the final results by adopting the more realistic model? It turns out that the choice between the two models is not just a matter of accuracy, since using the random coil model would lead to completely erroneous results for large networks. The reason behind this phenomenon is the asymptotic behaviour of the models on increasingly large distance.

Let's consider a connected infinite network of monomers being homogeneously distributed in space. Two spheres of radii $p, p + \delta$, are centred at a selected monomer. The number of monomers positioned in the volume between the two spheres is proportional to δp^2 when $\delta \rightarrow 0$. Thus, for any small $\delta > 0$, the asymptotical behaviour of the reaction probability is given by,

$$\lim_{p \rightarrow \infty} \delta p^2 \Phi^*(A) = \infty,$$

$$\lim_{p \rightarrow \infty} \delta p^2 \Phi(A) = 0.$$

In other words, in a model equipped with $\Phi^*(A)$ (unlike $\Phi(A)$) the reaction probability increases for increasing distance between the reacting monomers. This eliminates the random coil model Φ^* as a proper candidate to be employed in simulations of infinite network.

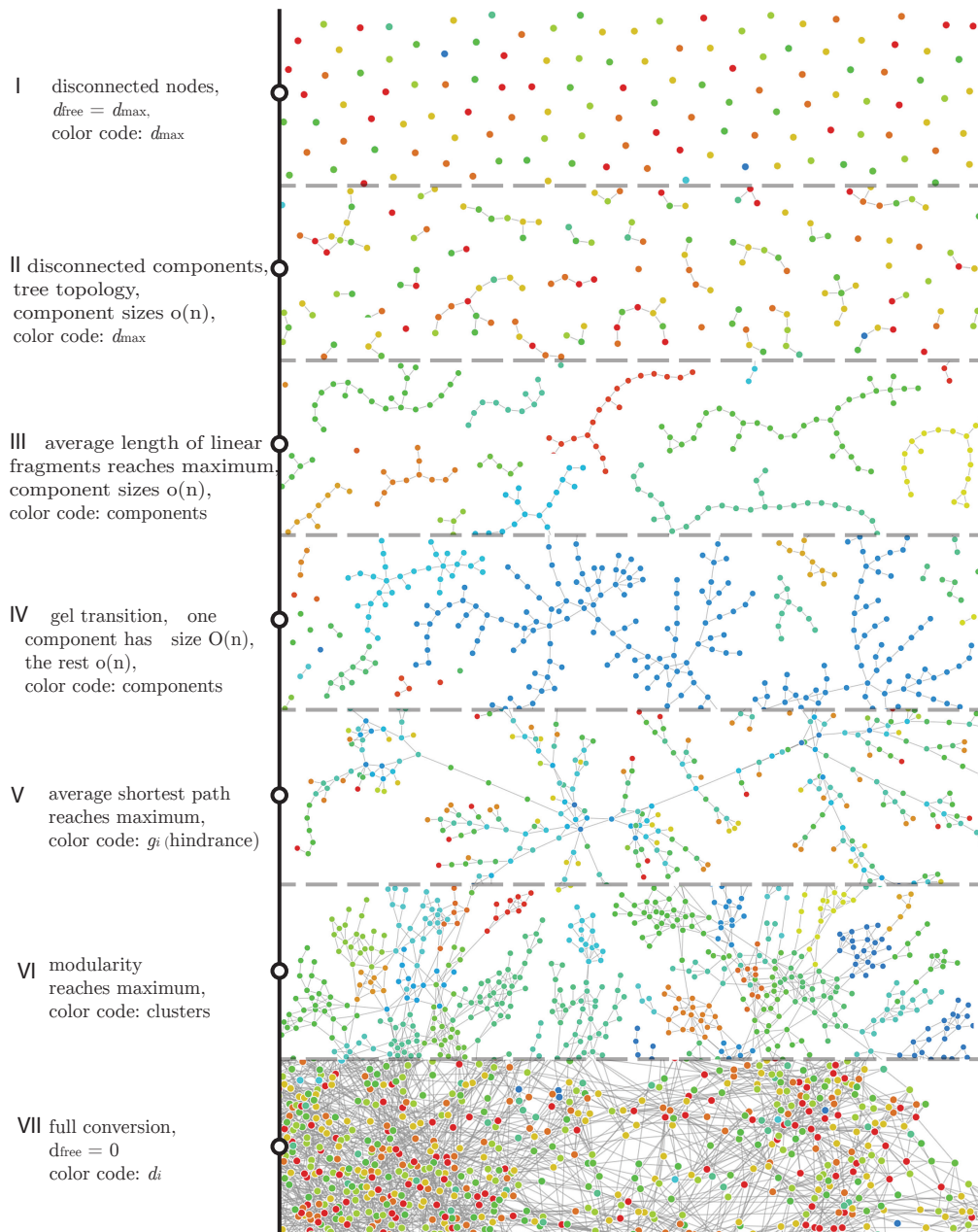


Figure 17: Timeline of network assembly, $k_c/k_p = 10$ (weak cyclisation)

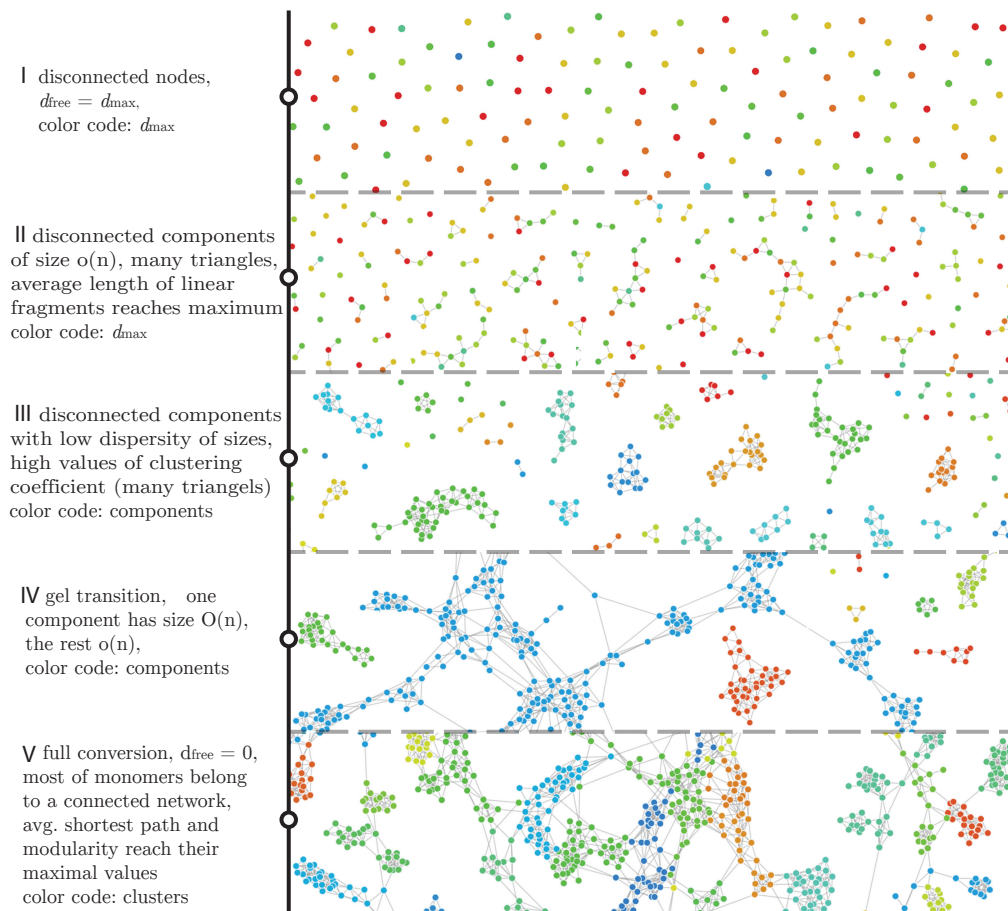


Figure 18: Timeline of network assembly, $k_c/k_p = 300$ (strong cyclisation)

5 Conclusions

We designed a new stochastic approach for modelling molecular networks that lies at the intersection of two disciplines: polymer reaction engineering and network science. The kinetics is accounted for by a Markov Chain accelerated Gillespie Monte Carlo routine. The main output is the network topology as presented by an adjacency matrix. Utilising adjacency matrices allows analyses with the whole ensemble of tools coming from graph theory: average shortest path, clustering, modularity, giant component transition, etc. These results are then used to estimate how the spatial position of monomers incorporated in the network affects their reactivity. The model turns out to reproduce polymer (network) characteristics like gel point transition, molecular size distributions, length of linear fragments. Additionally, the model gives insight into nuances of topological structure, for instance: the measure of non-homogeneity or cluster (micro-gel) distribution.

We have successfully applied the RGM algorithm to linseed oil polymerisation, more commonly known as the drying of oil paint. This process produces a TAG network that involves monomers of various functionality up 9, forming the building blocks the network. We showed that even though the degree distribution is fixed, as it is dictated by the natural abundance of fatty acids of different unsaturation in linseed oil, a wide range of different topologies emerge. Strong cyclisation (caused for instance by diluting the system) leads to highly non-homogeneous networks that are also less robust. In contrast, weak cyclisation causes more robust and homogenous structures.

If intra-monomeric reactions, that reduce functionality of monomers, take place even at a very slow rate they will considerably contribute to the final structure of the network in the post-gel regime, when rates of all other competing reactions are slowed down.

The resulting network topology is presented as an adjacency matrix, which allows employing graph theory oriented mechanical models to study elastic, transport, or rheological properties of the materials.

The main outcome of this work is an algorithm generating molecular topologies. However, alongside we have introduced a new vocabulary inspiring a new

way of discussing and comparing random molecular topologies, even regardless of the the methodology adopted to construct them.

Acknowledgement

This study has been funded by the PAinT (Paint Alterations in Time) project as part of the NWO (Dutch Science Foundation) Science4Arts Program. The authors (Jorien, Ivan, Joen, Piet) thank dr. Katrien Keune (Rijksmuseum/UvA), dr. Annelies van Loon (UvA), dr. Maartje Witlox-Stols (UvA), and Marta Mouro, MSc (UvA) for the inspiring discussions that have led to the problem formulation.

References

- [1] Yuki Akagi, Takuro Matsunaga, Mitsuhiro Shibayama, Ung-il Chung, and Takamasa Sakai. Evaluation of topological defects in tetra-peg gels. *Macromolecules*, 43(1):488–493, 2009.
- [2] David H Armitage, Colin Cameron, Allan H Fawcett, Cecil R Hetherington, Fred V McBride, and Richard AW Mee. Cycles within micronets and at the gel point. *Macromolecules*, 33(17):6569–6577, 2000.
- [3] Makoto Asai, Takuya Katashima, Ung-il Chung, Takamasa Sakai, and Mitsuhiro Shibayama. Correlation between local and global inhomogeneities of chemical gels. *Macromolecules*, 46(24):9772–9781, 2013.
- [4] David I Bower. *An introduction to polymer physics*. Cambridge University Press, 2002.
- [5] Steve Brooks, Andrew Gelman, Galin Jones, and Xiao-Li Meng. *Handbook of Markov Chain Monte Carlo*. CRC press, 2011.
- [6] Karel Dušek and Miroslava Dušková-Smrčková. Modeling of polymer network formation from preformed precursors. *Macromolecular Reaction Engineering*, 6(11):426–445, 2012.

- [7] Karel Dušek, Andrei Choukourov, Miroslava Duskova-Smrcková, and Hynek Biederman. Constrained swelling of polymer networks: Characterization of vapor-deposited cross-linked polymer thin films. *Macromolecules*, 47(13):4417–4427, 2014.
- [8] Karel Dušek, Miroslava Dušková-Smrcková, Jos Huybrechts, and Andrea Ďuračková. Polymer networks from preformed precursors having molecular weight and group reactivity distributions. theory and application. *Macromolecules*, 46(7):2767–2784, 2013.
- [9] Karel Dušek, Manfred Gordon, and Simon B Ross-Murphy. Graphlike state of matter. 10. cyclization and concentration of elastically active network chains in polymer networks. *Macromolecules*, 11(1):236–245, 1978.
- [10] RB Eggleton and Derek Allan Holton. *Graphic sequences*. Springer, 1979.
- [11] BE Eichinger. Embeddable random networks: method. *Polymer*, 46(12):4258–4264, 2005.
- [12] Paul J Flory. The configuration of real polymer chains. *The Journal of Chemical Physics*, 17(3):303–310, 1949.
- [13] Daniel T Gillespie. Stochastic simulation of chemical kinetics. *Annu. Rev. Phys. Chem.*, 58:35–55, 2007.
- [14] Michael D Goodner and Christopher N Bowman. Development of a comprehensive free radical photopolymerization model incorporating heat and mass transfer effects in thick films. *Chemical Engineering Science*, 57(5):887–900, 2002.
- [15] G Gündüz, M Dernaika, G Dikencik, M Fares, and L Aras. Graph theoretical approach to the mechanical strength of polymers. *Molecular Simulation*, 34(5):541–558, 2008.
- [16] Piet D. Iedema, Joen J. Hein, Katrien Keune, Annelies van Loon, and Maartje J.N. Stols-Witlox. Mathematical modeling of mature oil paint networks. In *ICOM-CC 17th Triennial Conference Preprints, Melbourne*, pages 1604–1612, 2014.

- [17] Dusanka Janezic, Ante Milicevic, Sonja Nikolic, and Nenad Trinajstic. *Graph-Theoretical Matrices in Chemistry*. CRC Press, 2015.
- [18] Dieter Jungnickel and Tilla Schade. *Graphs, networks and algorithms*. Springer, 2008.
- [19] Hendrik Kattner and Michael Buback. Chain-length-dependent termination of styrene bulk homopolymerization studied by sp- plp- epr. *Macromolecules*, 48(2):309–315, 2015.
- [20] I. Kryven and P. Iedema. Predicting multidimensional distributive properties of hyperbranched polymer resulting from ab_2 polymerization with substitution, cyclization and shielding. *Polymer*, 54:14:3472–3484, 2013.
- [21] I. Kryven and P. D Iedema. Topology evolution in polymer modification. *Macromolecular Theory and Simulations*, 23(1):7–14, 2014.
- [22] I. Kryven and P.D. Iedema. Deterministic modelling of copolymer microstructure: composition drift and sequence patterns. *Macromolecular Reaction Engineering*, page in press, 2014.
- [23] I. Kryven and P.D. Iedema. Transition into the gel regime for free radical crosslinking polymerisation in a batch reactor. *Polymer*, 55(16):3475–3489, 2014.
- [24] I. Kryven, S. Lazzari, and G. Storti. Population balance modeling of aggregation and coalescence in colloidal systems. *Macromolecular Theory and Simulations*, 23(3):170–181, 2014.
- [25] Michael Lang, Dietmar Göritz, and Stefan Kreitmeier. Length of subchains and chain ends in cross-linked polymer networks. *Macromolecules*, 36(12):4646–4658, 2003.
- [26] Michael Lang, Dietmar Göritz, and Stefan Kreitmeier. Intramolecular reactions in randomly end-linked polymer networks and linear (co) polymerizations. *Macromolecules*, 38(6):2515–2523, 2005.
- [27] Frank Lange, Konrad Schwenke, Manami Kurakazu, Yuki Akagi, Ungil Chung, Michael Lang, Jens-Uwe Sommer, Takamasa Sakai, and Kay

- Saalwächter. Connectivity and structural defects in model hydrogels: A combined proton nmr and monte carlo simulation study. *Macromolecules*, 44(24):9666–9674, 2011.
- [28] Stefano Lazzari, Shaghayegh Hamzehlou, Yuri Reyes, Jose Ramon Leiza, Mário Rui PFN Costa, Rolando Dias, and Giuseppe Storti. Bulk crosslinking copolymerization: Comparison of different modeling approaches. *Macromolecular Reaction Engineering*, 2014.
- [29] Erlita Mastan, Xiaohui Li, and Shiping Zhu. Modeling and theoretical development in controlled radical polymerization. *Progress in Polymer Science*, 45:71–101, 2015.
- [30] Mark Newman. *Networks: an introduction*. Oxford University Press, 2010.
- [31] Mark EJ Newman. Modularity and community structure in networks. *Proceedings of the National Academy of Sciences*, 103(23):8577–8582, 2006.
- [32] KL Ngai and CM Roland. Junction dynamics and the elasticity of networks. *Macromolecules*, 27(9):2454–2459, 1994.
- [33] D.H. Rouvray and R.B. King. *Topology in chemistry: Discrete mathematics of molecules*. Elsevier, 2002.
- [34] K Schwenke, M Lang, and J-U Sommer. On the structure of star-polymer networks. *Macromolecules*, 44(23):9464–9472, 2011.
- [35] Sebastian Seiffert and Mitchell Anthamatten. *Supramolecular Polymer Networks and Gels*, volume 268. Springer, 2015.
- [36] Joel Spencer. The giant component: The golden anniversary. *Notices of the AMS*, 57(6):720–724, 2010.
- [37] Lin Wang and Linda J Broadbelt. Explicit sequence of styrene/methyl methacrylate gradient copolymers synthesized by forced gradient copolymerization with nitroxide-mediated controlled radical polymerization. *Macromolecules*, 42(20):7961–7968, 2009.

- [38] Lin Wang and Linda J Broadbelt. Factors affecting the formation of the monomer sequence along styrene/methyl methacrylate gradient copolymer chains. *Macromolecules*, 42(21):8118–8128, 2009.
- [39] Ming Chen Wang and Eugene Guth. Statistical theory of networks of non-gaussian flexible chains. *The Journal of Chemical Physics*, 20(7):1144–1157, 1952.
- [40] Huaxing Zhou, Jiyeon Woo, Alexandra M Cok, Muzhou Wang, Bradley D Olsen, and Jeremiah A Johnson. Counting primary loops in polymer gels. *Proceedings of the National Academy of Sciences*, 109(47):19119–19124, 2012.